

Research Letter



Enabling 3D printing of carbons by polyethylene precursors

Paul Smith, Ethan Bounds, Kaleb Jones, Anthony Griffin, Zoe Gunter, Zhe Qiang¹⁰, School of Polymer Science and Engineering, The University of Southern Mississippi, 118 College Drive, Hattiesburg, MS 39406, USA

Address all correspondence to Zhe Qiang at zhe.qiang@usm.edu

(Received 29 April 2024; accepted 19 July 2024; published online: 29 July 2024)

Abstract

Development of low-cost and accessible techniques for creating intricate carbon structures is an important research area for advancing various applications. In this work, fused filament fabrication (FFF) of polyethylene (PE) is used to generate 3D-printed structures which are converted to carbon through sulfonation-induced crosslinking and subsequent pyrolysis. Carbons from PE precursors display more continuous morphologies than their polypropylene (PP) counterparts while achieving enhanced reaction kinetics at lower temperatures. This phenomenon enables robust mechanical properties under optimal carbonization conditions. This work provides an essential expansion of precursor selection and understanding of carbonization effects for 3D-printed carbon materials.

Introduction

Carbon materials have an indispensable role in the development of modern society. They are widely employed in various applications, including energy storage, [1] environmental remediation,^[2] thermal management,^[3] electronic devices,^[4] bioengineering, [5] and high-performance composites. [6] In general, carbon-based materials exhibit a combination of many advantageous physical properties, such as high electrical and thermal conductivity, mechanical strength, stiffness, as well as excellent thermal and chemical stability.^[7] Despite the wellestablished use and abundant nature of carbon, most technologies can only use these materials as a filler or additive within the presence of a matrix material. [8] Specifically, conventional methods face significant challenges in producing carbons into multi-dimensional structures without the presence of a matrix material. Typically, these matrix materials are polymeric and offer limited thermal stability. While it is possible to develop carbon matrices, their production is often constrained by timeconsuming and resource-intensive processes, which do not allow for intricate structural control. As a result, the ability to on-demand create complex and three-dimensional (3D) carbononly structures is still limited. In recent years, several additive manufacturing (AM, or 3D printing) methods have been developed to address this important need. Major approaches include the extrusion of highly filled carbon slurries or thermoplastics followed by matrix removal, and the AM of polymeric carbon precursors followed by direct pyrolysis. For example, extrusion approaches often employ direct ink writing (DIW) of aqueous slurries containing carbon nanomaterials such as graphene oxide deposited through a nozzle one layer at a time to create a structure. [9] Structures produced in this way then undergo solvent/matrix removal, yielding a carbonaceous structure. However, this method requires ink with specific thixotropic properties, which can be challenging to attain and optimize for

different systems, often demanding the use of fillers and process optimization to achieve desired printability. Recent work from Fu and co-workers has employed a similar approach using FFF of polylactic acid (PLA) filled with high concentrations of carbon nanotubes. [10] These printed structures then undergo matrix removal by thermal decomposition leaving fully carbonaceous structures. While these approaches are suited for preparing functional carbon structures with high surface area, the development of void space from matrix removal can lead to weakened mechanical properties. [11,12] Moreover, the use of highly engineered nanomaterials might be cost prohibitive for scaling up.

Alternatively, high char-yield resins can be printed into structured polymer green bodies, which are then converted to carbon upon pyrolysis. For example, Long and co-workers demonstrated that photocurable polyimide precursors can be printed through UV-assisted DIW and vat photopolymerization (VP) methods. Following thermal treatment steps of imidization and pyrolysis, these parts were converted to well-defined monolithic carbons.[13] In addition, recent work from Lu and co-workers demonstrated the ability to manufacture 3D carbon lattices using a polyethylene glycol diacrylate (PEGDA) photocurable resin through steps of VP and pyrolysis. [14] The partial pyrolysis of printed scaffolds allowed the formation of deformable carbon structures with high specific strength and energy absorption capabilities. While these processes can yield carbon monoliths with satisfactory mechanical properties, printed products typically experience a large degree of shrinkage during post-treatment and pyrolysis, which can exceed 60% dimensionally. Furthermore, we note that most polymeric precursors for 3D-printing carbons reported so far have relatively limited commercial availability which can lead to challenges with scalability.



Recently, an innovative method was developed to convert commodity PP filament into structured carbon though the use of conventional FFF, a low-cost and highly accessible 3D-printing method. Specifically, printed polypropylene (PP) structures can be crosslinked using sulfuric acid at elevated temperatures through a crack-assisted diffusion mechanism. Fully crosslinked samples can then be carbonized to yield structured carbons.[15] Furthermore, by utilizing filaments containing chopped carbon fibers, near-net-shape dimensional accuracy and tunable mechanical properties may be achieved. [16] A principal advantage of this system is the use of low-cost, commercially available precursor filaments, making it highly transformative to other research labs, as well as potential industrial sectors. Notably, polyolefin materials including PP and polyethylene (PE) are the most common type of plastics in the world. In the early 1990s, Postema et al. demonstrated the feasibility of carbon fiber production using PE fibers;^[17] subsequently, this area was systematically investigated by several research groups.[18-20] We note that only recently has PE become an emerging material candidate for FFF printing; the historical challenge of low printing accuracy due to a high degree of shrinkage and warping upon sample cooling has now been addressed through a combination of molecular design, composition optimization, and printing techniques, including the use of print bed adhesives.^[21] However, the opportunity to convert 3D-printed PE into structured carbons has not been explored; addressing this gap can further enhance the power of polyolefin-derived carbon production by diversifying the material candidate selection.

Herein, we demonstrate the ability to transform FFF-printed PE parts to structured carbons through crosslinking and carbonization steps. Specifically, we elucidate the kinetics of the sulfonation-induced crosslinking reaction for a PE system and the evolution of physical morphology throughout the process, and determine the pore characteristics and amorphous nature of the resulting carbon. This method can be extended to bioderived PE precursors, to allow a more sustainable manufacturing approach. Furthermore, the influence of carbonization conditions, including temperature ramp and time on the compressive mechanical properties of 3D-printed carbon materials, is investigated. We note that PE-derived carbon products can exhibit strong mechanical performance, surpassing their counterparts converted from PP precursors, which can be attributed to significantly reduced amounts of cracks generated during crosslinking. This work enables a more diversified precursor selection for AM of carbons, while unraveling the role of precursor design for controlling the properties of final carbon parts upon pyrolysis.

Materials and methods *Materials*

98 wt% sulfuric acid was purchased from Fisher Scientific. Braskem FL300PE FFF filament was purchased from Dynamism and used throughout this study as a model material

system. Braskem FL600PE-BIO polyethylene filament (Bio-PE filament) and Braskem FL100PP polypropylene filament were also employed in this work. The thickness of all filaments was 2.85 mm. Deionized (DI) water was obtained by passing tap water through a Milli-Q IQ 7003 ultrapure lab water purification system from Millipore Sigma.

Methods for producing structure

3D-printed structures in this study were generated using an Ultimaker S3 FFF printer with an AA 0.4 print core. A model system of cubic gyroid structures with a dimension of 1.65 cm and an infill density of 20% (no top, bottom, or wall layers) was used to perform investigations on the sulfonation kinetics of PE precursors. Infill density refers to the internal structural density of a printed part, where 100% represents a completely solid part. Filaments were printed with a nozzle temperature of 225°C and a bed temperature of 80°C. Parts were printed with a 1 cm brim and Magigoo PE bed adhesive applied to increase bed adhesion and prevent warping. Furthermore, a printing speed of 20 mm/s was used alongside a fan speed of 50%. STL files for complex structures used in this study were obtained on Thingiverse.com under creative commons. After printing, samples were transferred to glass beakers and submerged in concentrated sulfuric acid for the sulfonation-crosslinking reaction. The beakers were placed in a preheated Thermo Scientific Thermolyne FB1415m muffle furnace under isothermal conditions for different amount of time. Specifically, PE parts were crosslinked at a temperature of 135°C. After sulfonation process, the glass beakers were removed and passively cooled to room temperature. Once cooled, acid was decanted, and any excess acid residual on the samples was removed through rinsing with DI water at least three times (confirmed using pH paper). Samples were then dried in a vacuum oven overnight prior to carbonization. Unless indicated otherwise, for a typical carbonization process, crosslinked parts were placed in an Across international TF1400 tube furnace under an N2 atmosphere at a heating rate of 1°C min⁻¹ to 600°C and, thereafter, 5°C min⁻¹ to 800°C.

Characterization methods

The mass of printed structures, parts after crosslinking, and carbonization were obtained using a balance to determine the mass again after crosslinking and carbon yield of the final products. Differential scanning calorimetry (DSC) was performed using a Discovery 250 (TA Instruments). A heat—cool—heat cycle was employed with an initial heating cycle from 20 to 220°C at a rate of 10°C min⁻¹ to remove the thermal history of samples. Subsequently, samples were cooled to 20°C at a rate of 5°C min⁻¹ and then heated back to 220°C at a rate of 10°C min⁻¹. Data analysis was performed using Trios software. The degree of crystallinity was determined by comparing the measured enthalpy of melting events to that of a theoretical value from 100% crystalline polymer, which is~293 J/g for PE.^[22] The insoluble fraction of crosslinked samples was determined

by comparing the initial mass to the final samples mass after extraction with hot xylenes at 120°C.

Scanning electron microscopy (SEM) was performed using a Zeiss Ultra 60 field emission with an accelerating voltage of 10 kV to track changes in sample morphology upon sulfonation and carbonization, respectively. X-ray photoelectron spectroscopy (XPS) analysis was performed using a Thermo-Fisher ESCALAB Xi+spectrometer equipped with a monochromatic Al X-ray source (1486.6 eV, ~400 μm diameter spot size). Measurements were performed using the standard magnetic lens mode and charge compensation. The base pressure in the analysis chamber during spectral acquisition was $\sim 4 \times 10^{-7}$ mBar. Spectra were collected at a take-off angle of 90° from the plane of the surface. The pass energy of the analyzer was set at 20 eV for high-resolution scans and 150 eV for survey scans, with energy resolutions of 0.1 eV and 1.0 eV, respectively. Binding energies were calibrated with respect to C1s at 285.3 eV. All spectra were recorded and analyzed using the Thermo Scientific Avantage software.

To understand the physical properties of PE-derived carbons, Raman spectroscopy was performed using a DXR3 spectrometer (Thermo-Fisher), with a laser operated at 532 nm and a 5 mW power. Liquid nitrogen physisorption was performed on PE-derived carbon using a Tristar II 3020 surface area and pore size analyzer from Micromeritics. The pore size distribution and micropore volume were calculated from the sorption isotherms using the Barrett-Joyner-Halenda (BJH) model and t-plot method, respectively, while surface area was determined through Brunauer-Emmett-Teller (BET) analysis. Compressive mechanical testing was performed using a mechanical test system (MTS) Insight test frame with a 10 kN load cell with compression platen in accordance with a modified ASTM D695 standard; a strain rate of 1 mm min⁻¹ was used. Compressive specimens used in this study were composed of a 30% infill density gyroid pattern with no top or bottom layers in a cube shape with a length of 2 cm. All mechanical test specimens were sulfonated for 24 h at the peak melting temperature of the respective polymer, and carbonization condition with various ramp rates and hold times were explored. For each dataset, at least three samples were tested and error bars represent one standard deviation. All compression samples were tested in the Z-direction, along the layer-to-layer building direction. The resulting mechanical property data were analyzed to identify compressive yield strength as the point of zero slope in the stress-strain curve followed by steep decline in measured stress, and compressive modulus as the initial slope of the linear elastic regime. Dimensional shrinkage between the printed parts and the final carbon structures was assessed through the measurement of the length, width, and height of each sample with calipers and calculating the percent reduction after carbonization. The Joule heating experiments of 3D-printed carbons were performed by connecting the carbons to a DC power supply (from Dr. Meter). The voltage was increased, and the temperature was measured using a thermal camera (from HTI) and/or a thermocouple until the equilibrium state was reached.

Results & discussion

Producing 3D-printed carbon through the FFF printing of polyolefins is an emerging method. To briefly describe our process, PE filament is first printed using FFF to generate a precursor structure. This structure is then submerged in concentrated sulfuric acid at 135°C to undergo sulfonationinduced crosslinking. This step enables PE to become thermally stabilized and serve as an efficient carbon precursor. [23,24] Crosslinked structures are then pyrolyzed under a nitrogen atmosphere to yield a carbonaceous product. In a previous work, PP was established for AM of carbon;^[15] this study further extends precursor selection to PE, which is the most abundant type of plastics in the world. We note that PE has been investigated as a potential candidate for economic carbon fiber production, but its use for on-demand manufacturing 3D-structured carbon is still underexplored. As the process of converting polymer to carbon is inherently tied to the progress of crosslinking reaction, it is important to develop an understanding of the sulfonation-induced crosslinking kinetics of FFF-printed PE systems. Here, a model system of cubic open-celled gyroid structures with 1.65 cm length in dimension was employed, which had a 20% infill density. These samples were crosslinked for a variety of times in concentrated sulfuric acid at 135°C. The selection of this temperature is associated with the melting point of PE, which is also around 135°C (Fig. S1). During the reaction, the PE chains are first functionalized with sulfonic acid groups; their subsequent departure enables the formation of unsaturated bonds, which can then form inter-molecular crosslinking through multiple addition and rearrangement reactions to generate a thermally stabilized structure. The simplified chemical transformation of linear PE chains to a crosslinked network and then carbon is summarized in [Fig. 1(a)]. [20]

Fourier transform infrared spectroscopy (FTIR) was used to monitor changes in the chemical composition of PE upon sulfonation. As shown in [Fig. 1(b)], bands centered at 2920 and 1470 cm⁻¹ can be observed in the as-printed PE samples, which correspond to the alkyl stretching and bending, respectively. After 2 h of sulfonation, the intensity of these C-H bands decreases, and the evolution of new bands can be observed. Specifically, a band at 3300 cm⁻¹, indicative of -OH stretching, can be observed, as well as a band at 1650 cm⁻¹ emerged, which corresponds to the presence of C=C bonds in polymer backbones. Moreover, bands at 1250 and 1000 cm⁻¹ can be found upon sulfonation for 2 h, they are associated with the functionalization of sulfonic acid groups on the PE backbone. After 12 h of reaction, it was found that alkyl stretching and bending vibrations associated with unfunctionalized PE were nearly fully diminished, while bands associated with -OH stretching, C=C bonds, and -SO₃H groups persisted after the formation of the crosslinked structure.

Upon sulfonation, a key indicator for understanding reaction progress in bulk, 3D-printed PE samples is change in



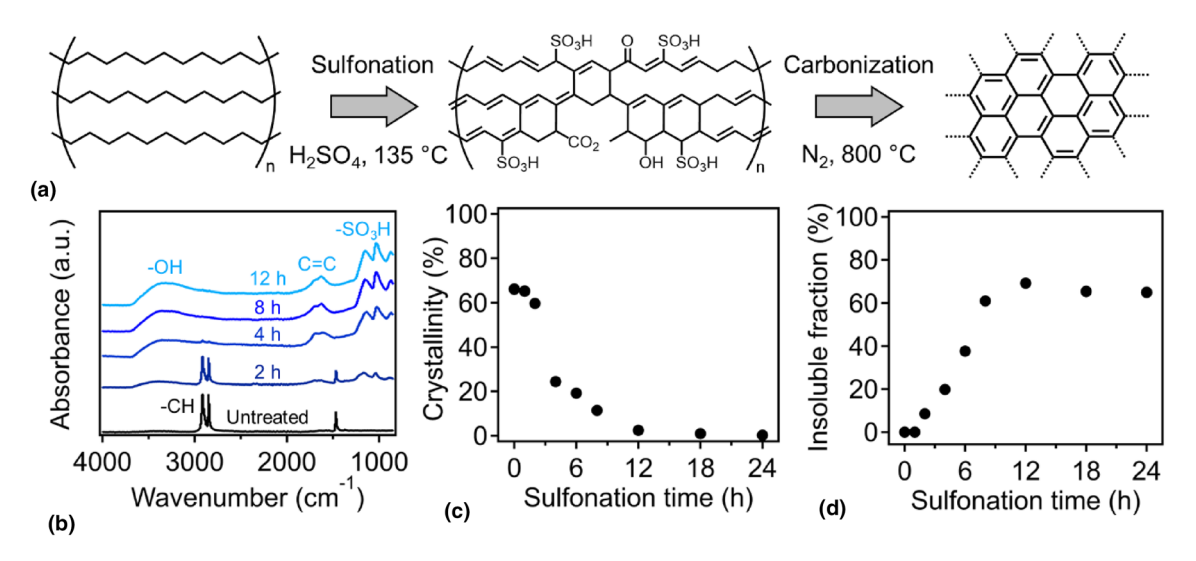


Figure 1. (a) A simplified illustration to demonstrate sulfonation-induced crosslinking mechanism of PE with sulfuric acid. (b) FTIR absorbance spectra versus sulfonation time of PE model system. (c) Changes in crystallinity of PE model system with increasing sulfonation time at 135°C. (d) Gel formation as monitored through mass of the insoluble fraction versus sulfonation time at 135°C.

their degree of crystallinity, which should decrease with increasing reaction time; the installment of functional groups and formation of networks limit the ability of polymer chains to (re)crystallize. Figure 1(c) shows the initial degree of crystallinity of PE, prior to sulfonation reaction, is approximately 65%, which quickly reduced to ~23% after only 4 h of reaction time. After 12 h, the sample only had a $\sim 2\%$ crystallinity degree. Raw DSC thermograms of sulfonated PE as a function of reaction time can be found in Fig. S1. Furthermore, the reaction kinetics observed from DSC measurements is consistent with the value of gel fraction content within the samples. Specifically, the gel content (insoluble fraction) is determined by the mass of samples after extraction with hot xylenes, which reach a plateau value of 62 wt% after 12 h, suggesting a completed crosslinking reaction of PE was achieved with the model system.

Previous work using PE and PP as precursors for carbon fiber (15–50 µm diameter) production found crosslinking reaction using sulfuric acid was a diffusion-controlled process. [25,26] However, for manufacturing carbons from FFF-printed PP parts, an important microcrack formation mechanism was observed. This behavior is attributed to the stress induced by mismatched volumetric expansion between outside part of layers (hydrophilic-sulfonated component) versus inside part (hydrophobic pristine component); the formation of cracks in the printed filaments facilitated acid diffusion and polymer crosslinking. A schematic representation of this process is depicted in Fig. 2(a). Using SEM, we found that similar microcrack channels were also present from the PE sulfonation reaction, as shown in Fig. 2(b-d). Specifically, Figure 2(b) depicts the structure of an untreated PE model specimen, noting the smooth and continuous structure composed of stacked layers characteristic of an FFF-printed part. After 2 h of sulfonation, [Fig. 2(c)], randomly oriented cracks can be observed to form

on the surface of the part. Upon extending the reaction time to 24 h, this cracked morphology is retained, as depicted in Fig. 2(d), without noticeable addition of cracks to the outer surface. We note that while the crosslinking temperature of PE in this work is lower than its counterpart of PP ($\sim 150^{\circ}$ C), cracks were found to occur at an earlier time (2 h vs 4 h for PP).

Interestingly, the morphology development of sulfonated/ crosslinked PE samples in this work was notably different from previous results of PP precursors. In addition to accelerated time to crack formation for PE, the number of cracks present in PE specimens was also reduced with a much greater crack-to-crack distance than their counterpart of PP, as shown in Fig. S2. The distinct cracking behavior between different polyolefin precursors can be attributed to following factors: (1) increased extensibility of PE, (2) lower reaction temperature, and (3) less rigorous sulfonation reaction in PE system due to the absence of tertiary carbon groups, which can lead to less chain scissions. Specifically, in the previous PP system, a sulfonation temperature of 150°C was employed, which was 5°C below the peak melting temperature of PP. In this study of PE, the sulfonation temperature was selected to be very close to the polymer melting temperature (135°C). As a result, the altered crosslinking condition influences the cracking phenomenon of polymer precursors significantly. At 135°C, PE was almost entirely devoid of crystalline domains, acting as a soft substrate during reaction. The increased portion of amorphous regions in PE precursors not only facilitates diffusion of sulfuric acid but also makes the substrate more tolerant to small degrees of deformation minimizing the formation of cracks. Collectively, these results confirm that the crosslinking of FFF-printed PE involves a crack-assisted diffusion mechanism.

Due to the crack-assisted diffusion of acid enabling PE crosslinking, a more than 60 wt% carbon yield can be obtained as shown in Fig. S3. Specifically, by increasing the sulfonation

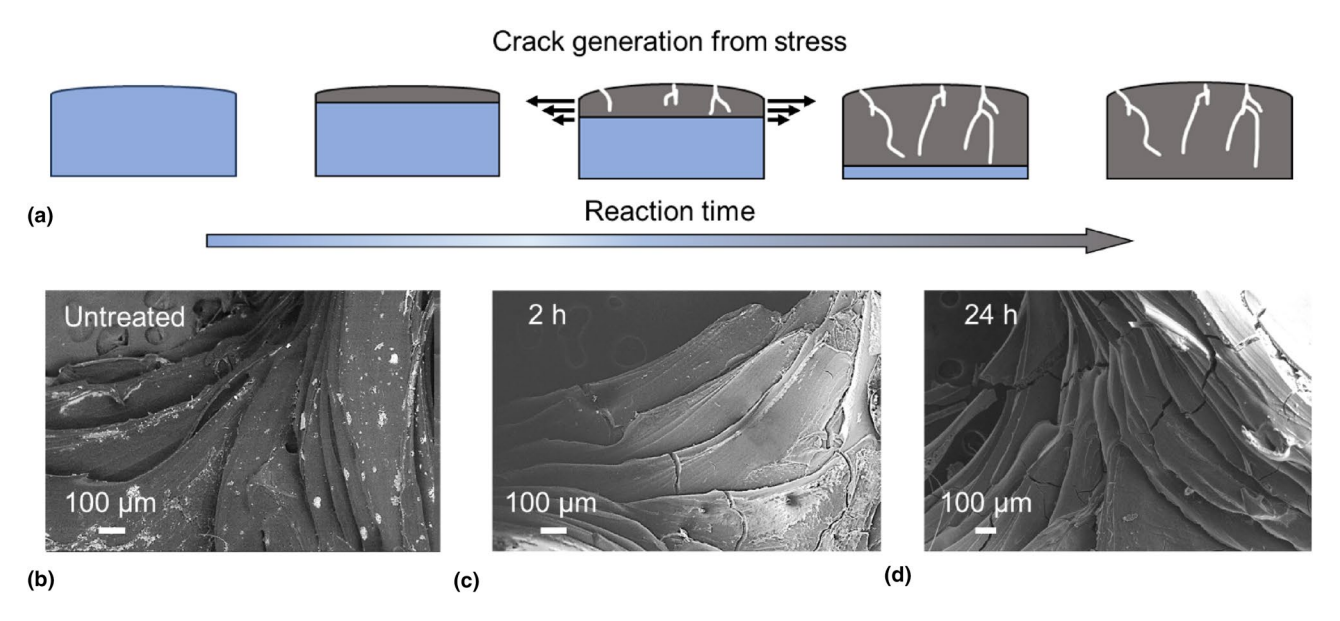


Figure 2. (a) Schematic representation of crack-assisted diffusion during sulfonation of thick PE parts. SEM images of (b) an uncrosslinked PE model specimen, (c) a specimen sulfonated for 2 h at 135°C, (d) a specimen sulfonated for 24 h at 135°C.

time from 2 to 8 and 12 h, the corresponding carbon yield of crosslinked PE increased from 0.3 to 53 wt% and 60 wt%, respectively. This result agreed well with observations of crosslinking kinetics presented in [Fig. 1(b-d)]. Completion of PE crosslinking within 12 h represents an important and necessary improvement in resource efficiency relative to PP sulfonated at 150°C which required at least twice amount of the time for full crosslinking to be achieved. Accelerated kinetics with reduced temperature requirements make PE a promising candidate for future study in optimized material systems for polyolefin-derived 3D-printed carbons. Moreover, as FFF is a highly industrially relevant AM technology, it is important to understand how our process proceeds with increased sample size and geometric complexity. Of particular interest, there is the dimensional shrinkage between the initial print and the final carbon structures as well as the corresponding carbon yield, given a single sulfonation condition. In this study, open-cell, cubic structures of 30% dense "gyroid" infill without top, bottom, or wall layers (depicted in Fig. S4) were printed at a range of sizes from 1 to 4 cm in length. These samples were all sulfonated for 24 h at 135°C. Figure 3(a) depicts the carbon yield and dimensional shrinkage of these samples as a function of their initial printed dimensions. Notably, due to the inherently anisotropic nature of FFF-printing process, these parts exhibit an average dimensional shrinkage of ~5% in Z-direction and a consistent value of ~ 19% in both X- and Y-directions. We note that the X- and Y-directions are functionally similar with deposited polymer aligned along the printing direction during extrusion, whereas the Z-direction is composed of a series of stacked layers. In turn, shrinkage in the X- and Y-directions was very similar, which was distinct from the behavior along the Z-direction. For all these samples, carbon yields were observed to be consistent at approximately 60–62 wt% across specimen

sizes under the same sulfonation condition. These results demonstrate that our reported approach can be employed to consistently produce large-scale 3D-printed carbon structures from PE.

After carbonization, the micro-scale morphology of these carbons was studied using SEM, as shown in [Fig. 3(b)]. These carbons were observed to retain their layered structure with the presence of microcracks, which were produced from the sulfonation reaction; there was no evidence showing more cracks were produced during pyrolysis. Figure 3(c) displays complex 3D-printed carbon structures manufactured through this technique, including a hexagonal grid structure, a highly complex "noodle" vase, and a columnar gyroid structure. These structures were observed to exhibit constant dimensional shrinkage below 20% in the XY-direction and ~8% in Z-direction (see Table S1 for details). The consistency in shrinkage and yield across different geometries suggests that this method is a versatile tool to manufacture complex 3D-printed carbons with reproducible dimensional accuracy.

Raman spectroscopy [Fig. 3(d)] was used to assess the physical nature of the PE-derived carbon framework. Peaks at ~1300 cm⁻¹ (I_d) and ~1550 cm⁻¹ (I_g) were both identified, corresponding to the disordered and graphitic fraction of carbons, respectively. The ratio of $I_d I_g$ is 1.36, indicating its largely amorphous structure, which is consistent with previous findings for polyolefin-derived carbon at a relatively low carbonization temperature (800°C). [27,28] Furthermore, to understand the pore textures of these carbons, liquid nitrogen physisorption was used in conjunction with BET and BJH analysis. The resulting type-II isotherm in [Fig. 3(e)] indicates a structure containing both macro- and micropores. Specifically, the BET surface area was found to be 634 m²/g with an average pore volume of 1.04 cm³/g; the formation of large amount of



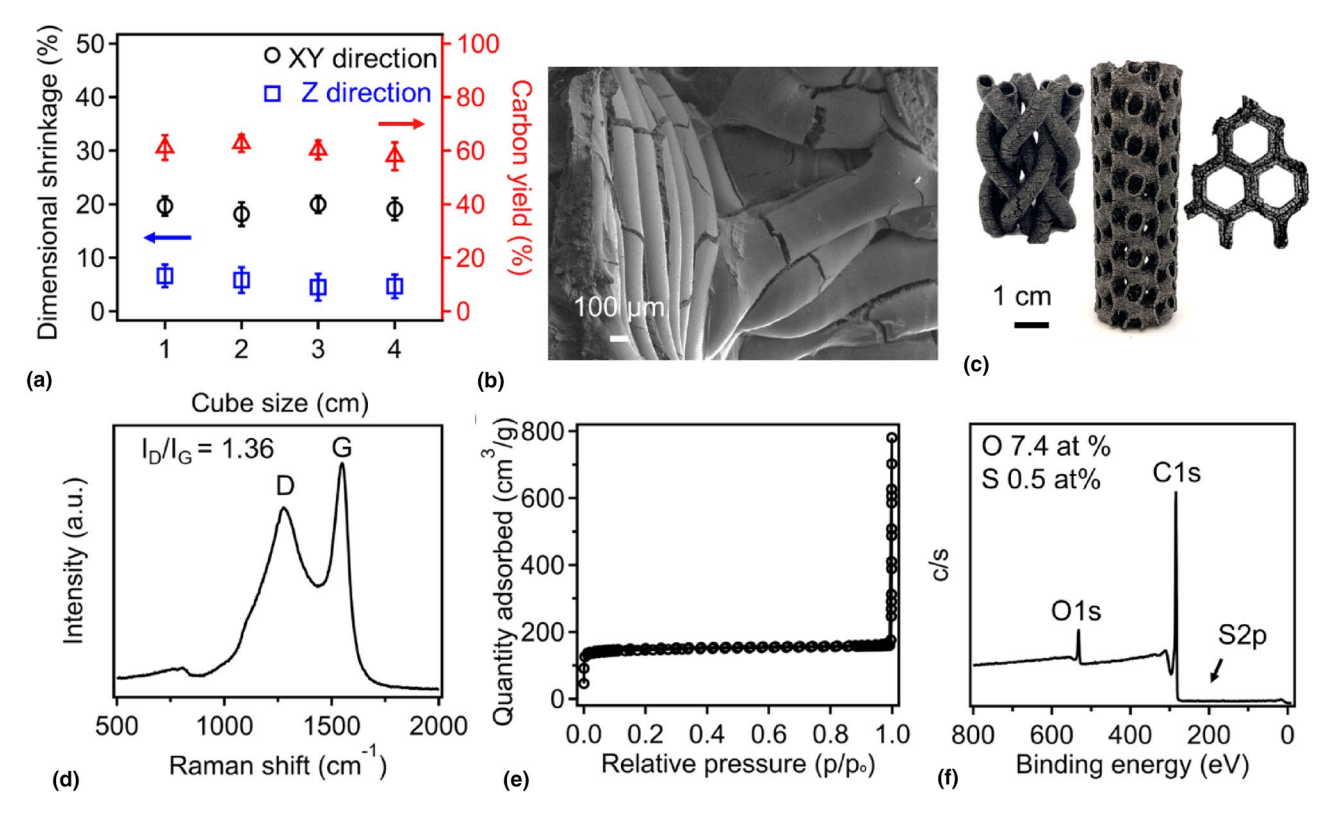


Figure 3. (a) Shrinkage and carbon yield of specimens ranging between 1 and 4 cm demonstrating process scalability. (b) SEM image showing the morphology of 3D-printed carbon derived from PE. (c) Complex carbon structures derived from PE, from left to right: hexagonal grid, "noodle" vase, columnar gyroid. (d) Raman spectra of PE-derived carbon with labeled peaks corresponding to disordered, D, and graphitic, G, contributions, the ratio of the area of these peaks is given as I_{α}/I_{g} and was found to equal 1.36. (e) BET isotherm of PE-derived carbon indicating a microporous structure. (f) XPS survey scan of PE-derived carbon, carbon, oxygen, and sulfur were identified.

micropores can be confirmed by their pore size distribution as shown in Fig. S5. Furthermore, as the crosslinking mechanism for PE involves the addition of sulfonic acid groups into polymer backbones and crosslinked networks, the resulting carbons can contain heteroatoms of both sulfur and oxygen. XPS [Fig. 3(e)] was used to determine the elemental composition of PE-derived carbons, where the survey scan indicated the presence of oxygen, carbon, and sulfur. High-resolution scans exploring the bonding state of carbon, oxygen, and sulfur are shown in Fig. S6(a-c) and the peaks associated with each bonding state are indicated. It was found that oxygen was present in the final carbons at 7.4 at% and sulfur heteroatom was observed at approximately 0.5 at%. We note that from high-resolution scans of C1s [Fig. S6(a)], C-C bonding states were most prevalent, while the presence of O–C–C and O–C=C bonding states were also observed. Furthermore, oxygen was determined to be present in both C-O and C=O states as suggested by fitted peaks centering at ~533 and ~531.5 eV, respectively, as shown in [Fig. S6(b)]. While the content of sulfur heteroatom in the carbon framework is relatively low, the co-presence of sulfur and oxygen in the carbon can be useful for altering material functionality; previous work show their enhanced performance in CO₂ capture, [29] and energy storage technology. [30]

Obtaining strong mechanical properties of these PE-derived carbon materials is a key factor in enabling their practical use. First, to demonstrate the versatility of this method to produce 3D-printed carbons, an additional precursor material, bioderived PE (bPE) produced from sugar cane, was investigated. This material was found to result in 3D-printed carbons with similar mechanical strength to the initial PE precursor given similar sulfonation and carbonization conditions, as shown in Fig. S7. To further develop an understanding of the influence of carbonization conditions on resulting mechanical properties of PE-derived carbons, a variety of samples were produced with the same geometry and sulfonation conditions (24 h at peak melting temperature) yet different carbonization profiles, informing optimal pyrolysis conditions. Specifically, samples composed of 30% infill density gyroid infill with no top, bottom, or wall layers were carbonized at heating rates of 0.5, 1, 5, and 10°C/min from room temperature to 800°C. In addition, a series of similar samples were produced following carbonization profiles with heating rates of 1°C/min from room temperature to 800°C with hold at maximum temperature ranging from 1 to 6 h.

Representative compressive stress-strain curves for these samples are reported in Fig. 4(a). From these results, it is

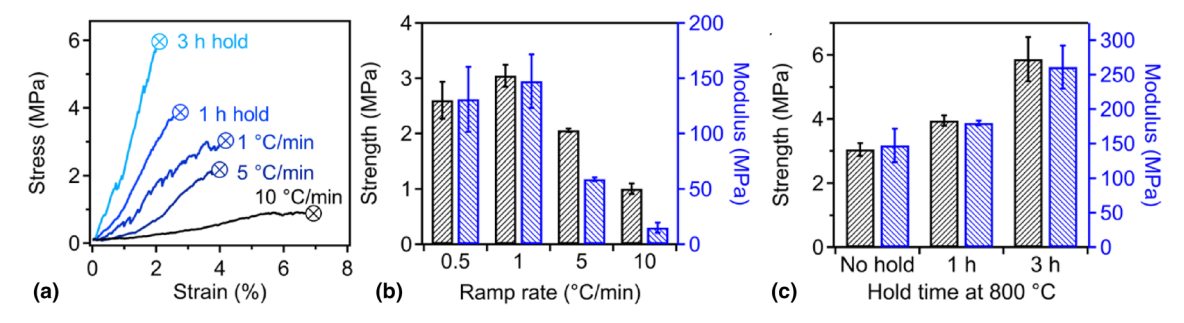


Figure 4. (a) Representative compressive stress–strain curves of bPE samples carbonized under selected conditions, samples indicated to have isothermal holds were prepared at a 1°C/min ramp rate. (b) Resultant mechanical properties of bPE carbon specimens as a function of carbonization ramp rate. (c) Resultant mechanical properties of bPE carbon specimens as a function of hold times during carbonization.

apparent that a reduction in ramp rate led to stronger mechanical properties in these materials, where increases in both modulus and ultimate strength may be observed. Specifically, as presented in [Fig. 4(b)], it was found that at a ramp rate of 0.5°C/min, samples exhibited an average strength of 2.6 ± 0.3 MPa and a modulus of 130 ± 29 MPa. These values were observed to diminish significantly upon increasing ramp rate. With a carbonization ramp rate of 5°C/min, compressive strength and modulus of derived carbon were reduced to 2.1 ± 0.03 MPa and to 59 ± 1.7 MPa, respectively. A further reduction occurred when the rate increased to 10°C/min where a strength of just 1.0 ± 0.1 MPa and a modulus of 15 ± 4.6 MPa were obtained. Raw mechanical traces for these carbons are additionally provided in Fig. S8(a-d). We attribute the differences in the mechanical properties of carbons obtained from various carbonization ramp rates to their distinct carbon yields. Specifically, as shown in Fig. S9, while ramp rates of 1 and 0.5°C/min result in a similar carbon yield of approximately 55 wt%, higher ramp rates of 5 and 10°C/min decrease the carbon yield to approximately 51 and 47 wt%, respectively. These results suggest that faster ramp rates can lead to the formation of softer and weaker carbon. Moreover, it is also likely that rapid polymer-to-carbon transformations result in the formation of an increased number of defects and prohibit adequate densification to produce strong and stiff carbons; these observations are consistent with carbon fiber production using PE precursors, where a higher-temperature ramp during pyrolysis may encourage more void formation and weakened mechanical performance.[23]

Furthermore, the influence of carbonization time at peak temperature on the resultant mechanical properties of these carbons were evaluated and the results are presented in Fig. 4(c). Raw compressive mechanical traces for these samples are given in Fig. S10(a–c). It was found that incorporating an isothermal hold of 1 h at 800°C led to a marked increase in both compressive strength and modulus. Samples increased in strength from 3.0 ± 0.2 MPa (without a hold) to 3.95 ± 0.2 MPa after 1 h and further strengthened to 5.9 ± 0.7 MPa after 3 h. Moreover, without a hold, an initial modulus of 147 ± 24 MPa was observed,

and this value could increase to 180±3 MPa after 1 h, and further increase to 261±31 MPa after 3 h. It is likely that this notable strengthening and stiffening were the result of increased densification of the carbonaceous structure during extended isothermal holds, which surpasses PP-derived, 3D-printed carbons with similar geometry.^[15] To further demonstrate the practical use of these 3D-printed carbons derived from PE precursors, additional experiments were conducted to showcase their excellent Joule heating performance, which is crucial for producing thermal energy with reduced energy consumption. In [Fig. S11(a)], a 3D-printed carbon structure reaches temperatures high enough to induce a glowing effect when exposed to 25 W of power. In addition, Fig. S11(b) presents a graph depicting the temperature versus power relationship, highlighting the highly efficient Joule heating performance of these carbons, such as reaching 400°C with just 15 W of power. These results suggest that carbon derived from PE precursors would be well suited to heating applications, while confirming the potential of using PE precursor to create structurally complex carbons with excellent mechanical properties. This work using 3D-printing technology enables the creation of complex carbon structures with high structural precision and low-cost materials, overcoming the limitations of traditional methods. This advancement not only simplifies the production process but also enhances the practical applications of these carbon materials, particularly in areas requiring efficient thermal management and energy use.

Conclusion

3D-printed structures generated from FFF printing of commercial PE filaments can serve as efficient carbon precursors through crosslinking with concentrated sulfuric acid. Crosslinking of printed PE structures proceeds through a crack-assisted diffusion process similar to PP precursors with improved reaction kinetics. We note that compared to PP, crosslinking of 3D-printed PE parts leads to less cracking, yielding a more continuous carbon structure. Upon pyrolysis, crosslinked PE structures can be converted to carbon with a reproduceable yield of over 60%. This process can be scaled to large and



complex structures with consistent shrinkage and carbon yield behaviors. Carbon resulting from this process is amorphous and microporous, containing oxygen and sulfur heteroatoms. In addition, this method can be extended to bio-derived PE filaments as the starting materials. The impact of carbonization profiles on the mechanical properties of the resulting carbon is systematically studied. Under optimal carbonization conditions, the mechanical properties of PE-derived carbons can be significantly better than their counterparts from PP precursors. Overall, this work demonstrates the ability to generate strong, functional 3D-printed carbons through low-cost PE precursors and a simple process.

Acknowledgments

The authors thank Jeffrey Aguinaga and Dr. Derek Patton for their support of XPS measurements.

Author contributions

P.S and Z.Q. were responsible for experiment design during this project. Majority of the experiments were carried out by P.S. with assistance from E.B., A.G, K. J., and Z. G. This manuscript was primarily written by P.S. and Z.Q., while all authors contributed. Z.Q. supervised all work through this project.

Funding

The authors acknowledge the financial support from National Science Foundation under the grant CMMI-2239408, and Depart of Energy under the grant DE-FE-0032280.

Data availability

Data of this work are available from the corresponding author based upon reasonable request.

Declarations

Conflict of interest

On behalf of all authors, the corresponding author states that there is no conflict of interest.

Supplementary Information

The online version contains supplementary material available at https://doi.org/10.1557/s43579-024-00619-3.

References

- J. Xiao, J. Han, C. Zhang, G. Ling, F. Kang, Q.H. Yang, Adv. Energy Mater. 12, 2100775 (2022)
- Y. Lan, Q. Du, C. Tang, K. Cheng, F. Yang, J. Environ. Manag. 296, 113340 (2021)
- A.A. Balandin, Nat. Mater. **2011**(10), 569–581 (2011)
- J. Khan, S.A. Momin, M. Mariatti, Carbon N. Y. 168, 65–112 (2020)
- W. Xu, S.K. Paidi, Z. Qin, Q. Huang, C.H. Yu, J.V. Pagaduan, M.J. Buehler, I. Barman, D.H. Gracias, Nano Lett. 19, 1409-1417 (2019)
- T.K. Das, P. Ghosh, N.C. Das, Adv. Compos. Hybrid Mater. 2, 214–233 (2019)

- 7. I. Edwards, H. Marsh, R. Menendez, S. West, A. Hosty, K. Kuo, B. McEnaney, T. Mays, D. Johnson, J. Patrick, D. Clarke, J. Crelling, R. Gray, Introduction to carbon science (Butterworth & Co., 1989)
- 8. A. Ramanathan, V. Thippanna, A.S. Kumar, B. Sundaravadivelan, Y. Zhu, D. Ravichandran, S. Yang, K. Song, J. Polym. Sci. (2023). https://doi.org/10.1002/POL. 20230632
- Q. Zhang, F. Zhang, S.P. Medarametla, H. Li, C. Zhou, D. Lin, Small 12, 1702-
- 10. C. Zhang, B. Shi, J. He, L. Zhou, S. Park, S. Doshi, Y. Shang, K. Deng, M. Giordano, X. Qi, S. Cui, L. Liu, C. Ni, K.K. Fu, Adv. Mater. 35, 2208230 (2023)
- 11. P. Blyweert, V. Nicolas, V. Fierro, A. Celzard, Carbon N. Y. 183, 449-485 (2021)
- 12. Y.M. Eggeler, K.C. Chan, Q. Sun, A.D. Lantada, D. Mager, R. Schwaiger, P. Gumbsch, R. Schröder, W. Wenzel, J.G. Korvink, M. Islam, Adv. Funct. Mater. 34, 2302068 (2023)
- 13. C.B. Arrington, D.A. Rau, J.A. Vandenbrande, M. Hegde, C.B. Williams, T.E. Long, ACS Macro Lett. 10, 412-418 (2021)
- 14. J.U. Surjadi, Y. Zhou, S. Huang, R.H.W. Lam, Z. Wang, Y. Lu, Matter (2022). https://doi.org/10.1016/j.matt.2022.08.010
- 15. P. Smith, A.G. Obando, A. Griffin, M. Robertson, E. Bounds, Z. Qiang, P. Smith, A.G. Obando, A. Griffin, M. Robertson, E. Bounds, Z. Qiang, Adv. Mater. 35, 2208029 (2023)
- 16. P. Smith, J. Hu, A. Griffin, M. Robertson, A. Güillen Obando, E. Bounds, C.B. Dunn, C. Ye, L. Liu, Z. Qiang, Nat. Commun. 15, 1-12 (2024)
- 17. A.R. Postema, H. De Groot, A.J. Pennings, J. Mater. Sci. 25, 4216–4222 (1990)
- 18. J.M. Younker, T. Saito, M.A. Hunt, A.K. Naskar, A. Beste, J. Am. Chem. Soc. (2013). https://doi.org/10.1021/ja3121845
- 19. M.J. Behr, B.G. Landes, B.E. Barton, M.T. Bernius, G.F. Billovits, E.J. Hukkanen, J.T. Patton, W. Wang, C. Wood, D.T. Keane, J.E. Rix, S.J. Weigand, Carbon (2016). https://doi.org/10.1016/j.carbon.2016.06.032
- 20. B.E. Barton, J. Patton, E. Hukkanen, M. Behr, J.-C. Lin, S. Beyer, Y. Zhang, L. Brehm, B. Haskins, B. Bell, B. Gerhart, A. Leugers, M. Bernius, Carbon (2015). https://doi.org/10.1016/j.carbon.2015.07.029
- 21. C.G. Schirmeister, T. Hees, E.H. Licht, R. Mülhaupt, Addit. Manuf. 28, 152–159 (2019)
- J.D. Menczel, R.B. Prime, Thermal analysis of polymers: fundamentals and applications (Wiley, Hoboken, 2008), p.111
- 23. T. Röding, J. Langer, T. Modenesi Barbosa, M. Bouhrara, T. Gries, App. Res. 1, e202100013 (2022)
- 24. A.G. Obando, M. Robertson, C. Umeojiakor, P. Smith, A. Griffin, Y. Xiang, Z. Qiang, J. Mater. Res. 39, 115-125 (2024)
- 25. A. Griffin, P. Smith, P. Frame, K. Jones, Z. Qiang, Adv. Sustain. Syst. 8, 2300332
- 26. C.A. Marcus Hunt, T. Saito, R.H. Brown, A.S. Kumbhar, A.K. Naskar, M.A. Hunt, T. Saito, R.H. Brown, A.K. Naskar, A.S. Kumbhar, Adv. Mater. 24, 2386–2389
- 27. B.E. Barton, E.J. Hukkanen, G.F. Billovits, D. Schlader, M.J. Behr, D. Yancey, M. Rickard, X. Qiu, D.M. Mowery, L. Brehm, B. Haskins, W. Wang, M.S. Spalding, C. Derstine, Carbon (2018). https://doi.org/10.1016/j.carbon.2018.01.031
- 28. B. Laycock, X. Wang, R.F. Liu, P.K. Annamalai, J. Cork, C. Derstine, M. Mills, E.W. McFarland, Polym. Degrad. Stab. 172, 109057 (2020)
- 29. M. Robertson, A.G. Obando, B. Nunez, H. Chen, Z. Qiang, A.C.S. Appl, Eng. Mater. 1. 165-174 (2022)
- 30. L. Qie, W. Chen, X. Xiong, C. Hu, F. Zou, P. Hu, Y. Huang, L. Qie, W. Chen, X. Xiong, C. Hu, F. Zou, P. Hu, Y.H. Huang, Adv. Sci. (2015). https://doi.org/10.1002/ADVS. 201500195

Publisher's Note Springer Nature remains neutral with regard to jurisdictional claims in published maps and institutional affiliations.

Springer Nature or its licensor (e.g. a society or other partner) holds exclusive rights to this article under a publishing agreement with the author(s) or other rightsholder(s); author self-archiving of the accepted manuscript version of this article is solely governed by the terms of such publishing agreement and applicable law.